SAND2022-5506C

Carbon Dioxide Seeding System for Enhanced Rayleigh Scattering in Sandia's Hypersonic Wind Tunnel

Ashley J. Saltzman*, Steven J. Beresh†, Katya M. Casper‡, Brian P. Denk§, Rajkumar Bhakta**, Marie E. De Zetter††, and Russell W. Spillers‡‡
Sandia National Laboratories, Albuquerque, New Mexico 87185

This work describes the development and testing of a carbon dioxide seeding system for the Sandia Hypersonic Wind Tunnel. The seeder injects liquid carbon dioxide into the tunnel, which evaporates in the nitrogen supply line and then condenses during the nozzle expansion into a fog of particles that scatter light via Rayleigh scattering. A planar laser scattering (PLS) experiment is conducted in the boundary layer and wake of a cone at Mach 8 to evaluate the success of the seeder. Second-mode waves and turbulence transition were well-visualized by the PLS in the boundary layer and wake. PLS in the wake also captured the expansion wave over the base and wake recompression shock. No carbon dioxide appears to survive and condense in the boundary layer or wake, meaning alternative seeding methods must be explored to extract measurements within these regions. The seeding system offers planar flow visualization opportunities and can enable quantitative velocimetry measurements in the future, including filtered Rayleigh scattering.

I. Introduction

THE boundary layer and wake of a body in hypersonic flow play an important role in fluid-structure interaction. During boundary layer transition, high pressure fluctuations occur, which disturb the body and can cause vibrations. Additionally, the wake behind a hypersonic vehicle is unsteady and composed of recirculation regions, which can be a driver for these fluid-structure interactions. Historically, hypersonic boundary layer and wake measurements were

* Postdoctoral Appointee, Engineering Sciences Center, Member AIAA
† Distinguished Member of the Technical Staff, Engineering Sciences Center, Associate Fellow AIAA
‡ Principal Member of the Technical Staff, Engineering Sciences Center, Associate Fellow AIAA
§ Technologist, Engineering Sciences Center
** Senior Test Operations Engineer, Engineering Sciences Center
†† Technologist, Engineering Sciences Center
‡‡ Principal Technologist, Engineering Sciences Center

made using pressure rakes, Pitot probes, or hot wire anemometry [1]. As these instruments inherently interfere with the flow, it is desired to characterize these complex flow fields using robust, non-intrusive techniques.

Hypersonic flow presents a challenging testing environment for most modern diagnostics. Common flow visualization techniques, such as schlieren or shadowgraph, integrate spatially through the flow and thus can be misleading for highly three-dimensional flows. These techniques may also struggle in the low-density environments found in high Mach number flows as high measurement sensitivity is needed. Planar velocimetry techniques, such as particle image velocimetry (PIV) and Doppler global velocimetry (DGV), require particles to be added to the flow to scatter light and determine velocity. In a hypersonic flow, these Mie scattering based diagnostics are unsuitable due to concerns of particle lag. However, light can also be scattered by particles much smaller than the laser's wavelength, the Rayleigh regime. Molecules within the flow are small enough to accurately trace the flow and scatter light via Rayleigh scattering. This scattered light will experience a Doppler shift based on the velocity of the flow, which can be distinguished using a molecular filter, in a technique known as Filtered Rayleigh Scattering (FRS). While FRS can provide information on velocity, temperature, pressure, and density, molecular Rayleigh scattering is weaker than Mie and background scattering and can be difficult to detect in low-density flows [2].

For super- and hypersonic flows, researchers have sought to enhance the amount of Rayleigh light scattering by not relying solely on molecular scattering. A small amount of carbon dioxide or alcohol is added to the flow, or tunnel dryers are turned off to keep water vapor in the supply, which condenses due to expansion from the nozzle in a technique known as condensate-enhanced Rayleigh scattering [3]. The fine fog of particles scatters light at different intensities, owing to changes in density or temperature and revealing turbulent structures and shocks. Previous efforts have resulted in, for example, visualizations of large-scale structures in supersonic shear layers [4, 5], wave instabilities on an elliptic cone in hypersonic flow [6], and turbulent boundary layers [7, 8] using scattering from condensed particles. Additionally, FRS and Mie-scattering-based DGV techniques are known to be well-suited to large measurement facilities, with quantitative velocity results demonstrated in the Subsonic Aerodynamic Research Lab (SARL, [9]), the National Full-Scale Aerodynamic Complex (NFAC) at NASA Ames [10], and the supersonic wind tunnel at NASA Langley [11].

Carbon dioxide is preferable for seeding systems over water or ethanol, as it has suitable evaporation and condensation behavior at the operating temperatures and pressures in hypersonic flows. Carbon dioxide is a gas at room temperature, meaning it will fully evaporate prior to entering tunnel heating sections, which can be damaged by

liquid droplets [12]. First demonstrated by Erbland et al. [13], carbon dioxide seeding systems for wind tunnels have previously been developed at Princeton University [3], Peking University [14], and Stanford University [15]. More recently, the United States Naval Academy used CO_2-enhanced Rayleigh scattering for characterization of their supersonic wind tunnel flow quality [16].

The current work seeks to add this seeding capability to the Sandia Hypersonic Wind Tunnel (HWT). The seeding system described herein has initially been developed and tested for Mach 8 flow, but it will eventually be updated to support Mach 5 operation. The success of the seeder is evaluated using a simple Planar Laser Scattering (PLS) setup, with comparisons to schlieren images. The boundary layer and wake of a sharp-nosed cone are visualized using PLS at a variety of Reynolds numbers. Through testing of the seeding system, detailed images of the boundary layer, wake structure, and turbulence transition are obtained and discussed in the current work. The paper is organized as follows: Sect. II provides details on the seeding system and experimental setup of the PLS and schlieren imaging systems, Sect. III shows resulting images in the wake and discusses obtained signal levels, and Sect. IV discusses the conclusions and future work.

II. Methods

A. CO_2 Seeding System and Facility

All testing was conducted in the Sandia Hypersonic Wind Tunnel (HWT). HWT is a blowdown-to-vacuum facility using interchangeable nozzles and heaters to enable test section Mach numbers of 5, 8, or 14. Only Mach 8 was used by the current work, which uses nitrogen gas as the working fluid and has a 355.6 mm diameter axisymmetric test section. The high-pressure nitrogen provides stagnation pressures ranging from 1720 to 6890 kPa, and the heater section provides stagnation temperatures ranging from 500 – 890 K. HWT is capable of run times up to 60 seconds long, with a 45-minute turnaround time between runs. Further details on the facility can be found in Refs. [12] and [17].

Successful demonstrations of enhanced Rayleigh scattering have been achieved using carbon dioxide (CO_2), ethanol, and water. To choose a gas for the seeder design, nucleation characteristics, phase characteristics, and risks to tunnel hardware were evaluated. Both water and ethanol have higher nucleation rates than CO_2 [18-20]. This suggests that ethanol or water would condense into larger particles, which may survive in hotter parts of the flow as seen by Ref. [7], while CO_2 will condense into a finer fog of particles. However, larger water or ethanol droplets, unlike CO_2, may not fully evaporate prior to entering the heating section, presenting a risk of damaging the heater

screens. Lastly, ethanol is highly flammable, presenting a risk for entering the heater section. Particles cannot be injected downstream of the heater due to space limitations upstream of the nozzle entrance. Back flow to the heater during shutdown would also pose a risk. Therefore, CO_2 was chosen for the design of the current system.

The CO_2 seeding system was first designed for application to Mach 8 flow and will eventually be modified to support Mach 5. A gaseous CO_2 seeding system was initially designed but did not perform well at this Mach number. At the required pressures and flow rates, the pressure drop was large enough to generate dry ice, resulting in frozen lines and valves. This occurrence was also observed by Erbland et al. at Mach 8 [13], but other groups operating at lower Mach numbers have had success with gaseous seeding systems [14, 16]. A liquid CO2 seeding system was therefore designed for application to HWT, shown in Fig. 1.

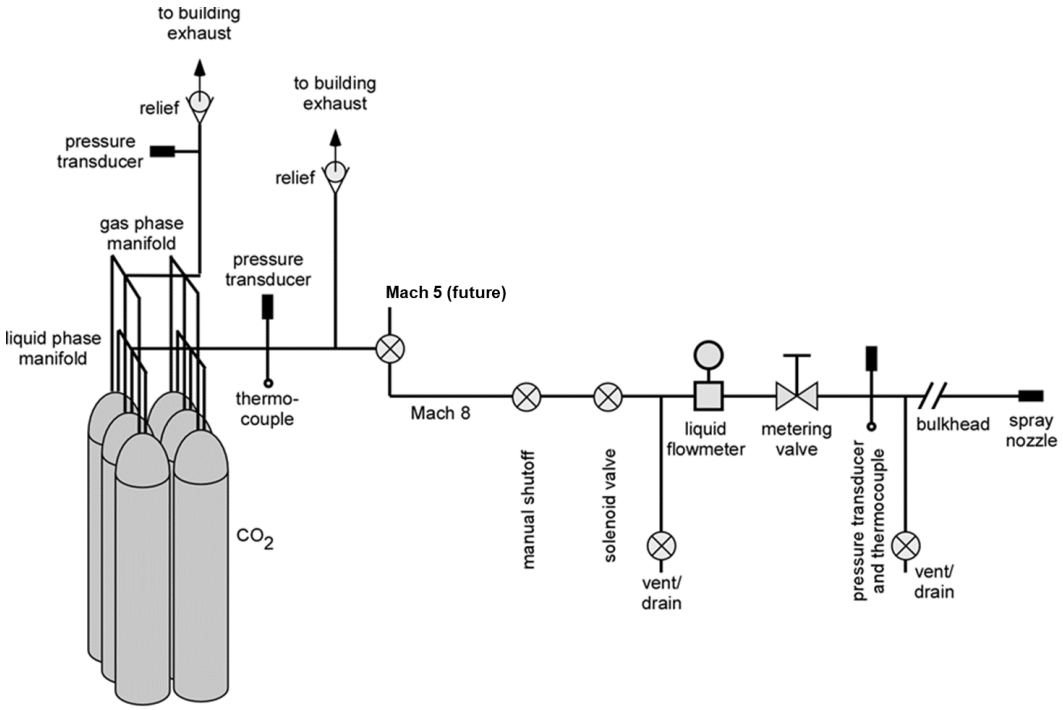

Fig. 1 Diagram of the carbon dioxide seeding system for the Sandia Hypersonic Wind Tunnel.

The liquid CO_2 is extracted from each of the six supply bottles using high pressure helium and an eductor tube. The seeder flow is metered manually using a needle valve, which is adjusted prior to each run depending on the specified wind tunnel conditions and the desired CO_2 quantity. This valve is located close to the spray nozzle to minimize expansion and temperature drop experienced by the CO_2. A spray nozzle breaks the liquid CO_2 into droplets as it is injected into the main nitrogen supply. Owing to the small droplet size and temperature, the CO_2 fully

evaporates before entering the heater and is then fully mixed through the heater section. With the nozzle expansion, the temperature decreases, causing the CO_2 to condense. Previous work by Hill [21] suggests the condensation mechanism in the nozzle is likely homogeneous nucleation, with average condensate sizes less than 100 nm [22]. If the temperature of the flow rises above the sublimation temperature of CO_2, as in the boundary layer or other hotter parts of the flow, the condensate sublimates, revealing the interface between cold and hot flow. A LabVIEW program controls the flow remotely via a 24V solenoid valve, in addition to monitoring the system temperature, pressure, and total flow rate during the tunnel run. The seeding system can supply approximately 2.7 gallons of liquid CO_2 per minute, approximately 1-2% by mass of HWT flow.

Several safety features were implemented into the design of the CO_2 seeder. Pressure relief valves are located throughout the system to prevent overpressure. Proper flow direction is assured with check valves at each bottle connection point and the final injection point, preventing backflow of nitrogen into the CO_2 system. Lastly, a CO_2 detector was installed in the room to alert personnel of levels exceeding 4000 ppm, preventing an asphyxiation hazard.

B. Imaging Experiment

For initial evaluation of the success of seeding the hypersonic tunnel, planar laser scattering (PLS) experiments were conducted and are depicted in Fig. 2. First, the boundary layer of a center sting-mounted, 7° half-angle, sharp-nosed cone with a base diameter of 127 mm was imaged using a single camera Fig. 2(a). Following this, a sharp-nosed, 5° half-angle cone with a base diameter of 76.1 mm was used with the interest of studying the wake flow. The cone is blade-mounted, rather than sting mounted, to provide minimal interference of the mounting of the model on the wake dynamics. The first wake PLS configuration looks at the area immediately downstream of the model base (near wake). In a second wake configuration, the laser sheet and cameras are positioned further downstream (far wake). A double-pulsed Nd:YAG laser (Quantel, Evergreen HP) was used for this experiment, providing 532 nm light with 300 mJ per pulse and pulse widths less than 10 ns. Each laser can be operated at rates up to 25 Hz; so, the two laser cavities were operated out of phase to enable a total repetition rate of 50 Hz in the current work. The laser beam is directed to the wind tunnel test section and expanded into a laser sheet using a cylindrical lens with a focal length of -10.1 mm. Using a converging lens with a focal length of 1.5 m, the laser sheet was focused to the measurement region of interest with a thickness of 0.8 mm. Two sCMOS cameras (PCO.edge 5.5) operating at a 50 Hz framerate were used to observe the CO_2-enhanced Rayleigh scattering. In the boundary layer, a single camera was used and fit with a Nikon 60 mm lens with an f-stop of 2.8. In the near wake, Camera 1 was fit with a Nikon 60 mm lens, while Camera

2 was fit with a 105 mm lens, both with f-stops of 2.8. In the far wake configuration, the cameras were each fit with Nikon 105 mm lenses with an f-stop of 2.8.

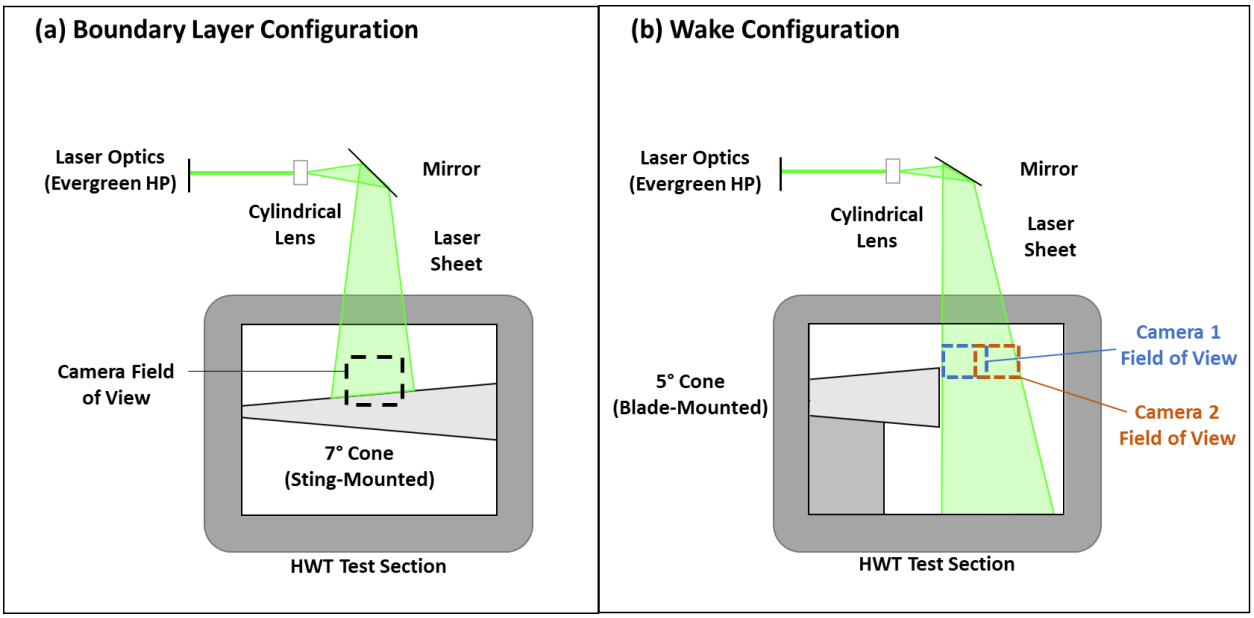

Fig. 2 Planar laser scattering experiment setup in the hypersonic wind tunnel from the cameras' perspective. (a) Measurement configuration observing the boundary layer. (b) Measurement configuration observing the wake. The laser sheet and cameras could be moved in this configuration to observe both the near and far wake. Diagram is not to scale.

A schlieren imaging system was also used for comparison to the PLS wake images. Although schlieren is a path-integrated measurement, flow structures may appear similar enough that comparison to PLS is feasible. During the schlieren runs, the CO_2 seeding system was not operated to ensure any observations were the result of the flow, and not the flow seeding. The Z-type schlieren system used a pair of 450.8 mm diameter spherical lenses for light collimation through the tunnel and a 300 mm lens for focusing light onto the sCMOS camera (PCO.edge 5.5) used for image acquisition at 50 Hz. A laser (Cavilux Smart UHS, 646 nm) was used as the schlieren light source, supplying 100 ns laser pulses at 50 Hz, synchronized with the camera frames. The schlieren images viewed a 200 × 200 mm^2 region downstream of the model, spanning both regions imaged by PLS with a resolution of 0.12 mm/pixel.

C. Flow Conditions

Several wind tunnel conditions varying in Reynolds number, *Re*, were used to characterize the seeder behavior, as well as provide an idea of the turbulence transition in the wake. The tunnel conditions and measurement configurations are summarized in Table 1, and all conditions were run at Mach 8. T_0 and P_0 refer to the tunnel stagnation temperature and pressure, respectively. Each 'X' in the table marks a separate wind tunnel run at the specified condition. The boundary layer at three Reynolds numbers was imaged using PLS. Four different Reynolds numbers were imaged using near wake PLS and full view schlieren. No far wake images were obtained for the highest Reynolds number, Run 4, due to screen damage within the heater section during the run. At this time, it is unclear if the screen was damaged as a result of using the CO_2 seeding system or due to normal wear on the wind tunnel heater.

Table 1 Summary of tunnel conditions and measurement configurations

Run Number	T_0 [K]	P_0 [kPa]	*Re* [1/m]	Boundary Layer PLS	Near Wake PLS	Far Wake PLS	Wake Schlieren
1	828	2068	4×10^6	X	X	X	X
2	606	2413	7×10^6		X	X	X
3	600	3654	10×10^6	X	X	X	X
4	611	4964	14×10^6	X		X	X

III. Results and Discussion

This section presents several images of the wake obtained during testing of the CO_2 seeding system. The image results are presented in three subsections to discuss the boundary layer, near wake, and far wake in detail. The images shown within this section have been post-processed to remove the background light using an average of 10 images taken immediately prior to the run, while the tunnel was at vacuum pressure. In total, 600 images were collected during each run by each PLS camera, and 1200 images were collected by the schlieren camera, in a separate set of runs.

A. Boundary Layer Results

Figure 3 shows resulting images from the first experimental configuration, to visualize the boundary layer along the cone, with the solid white line indicating the surface wall of the cone. The coordinate system places the origin at the center of the base of the model. Two instantaneous frames are shown for each Reynolds number, to highlight the variety of flow structures observed by PLS. The condensed CO_2 visualizes the freestream, as well as the conical shock from the model nose tip. Near the wall, the increased temperature sublimates the CO_2 particles, resulting in the distinctly visible boundary layer shown in Fig. 3. Figure 3(a) shows a canonical laminar boundary layer, while Fig.

3(b) shows clear second-mode disturbances. In the left column these disturbances appear to dissolve further downstream. In the right column, these disturbances grow into larger structures, indicating the boundary layer is transitioning to turbulence. This transition continues in the highest Reynolds number case, Fig. 3(c). In the left column, a fully turbulent boundary layer is apparent, while the right column appears to show a transition of the second mode waves to turbulence. With this PLS configuration, a large amount of background light impacted the image quality due to scattering off the model's surface. Signal levels will be discussed in more detail in Sect. IIID.

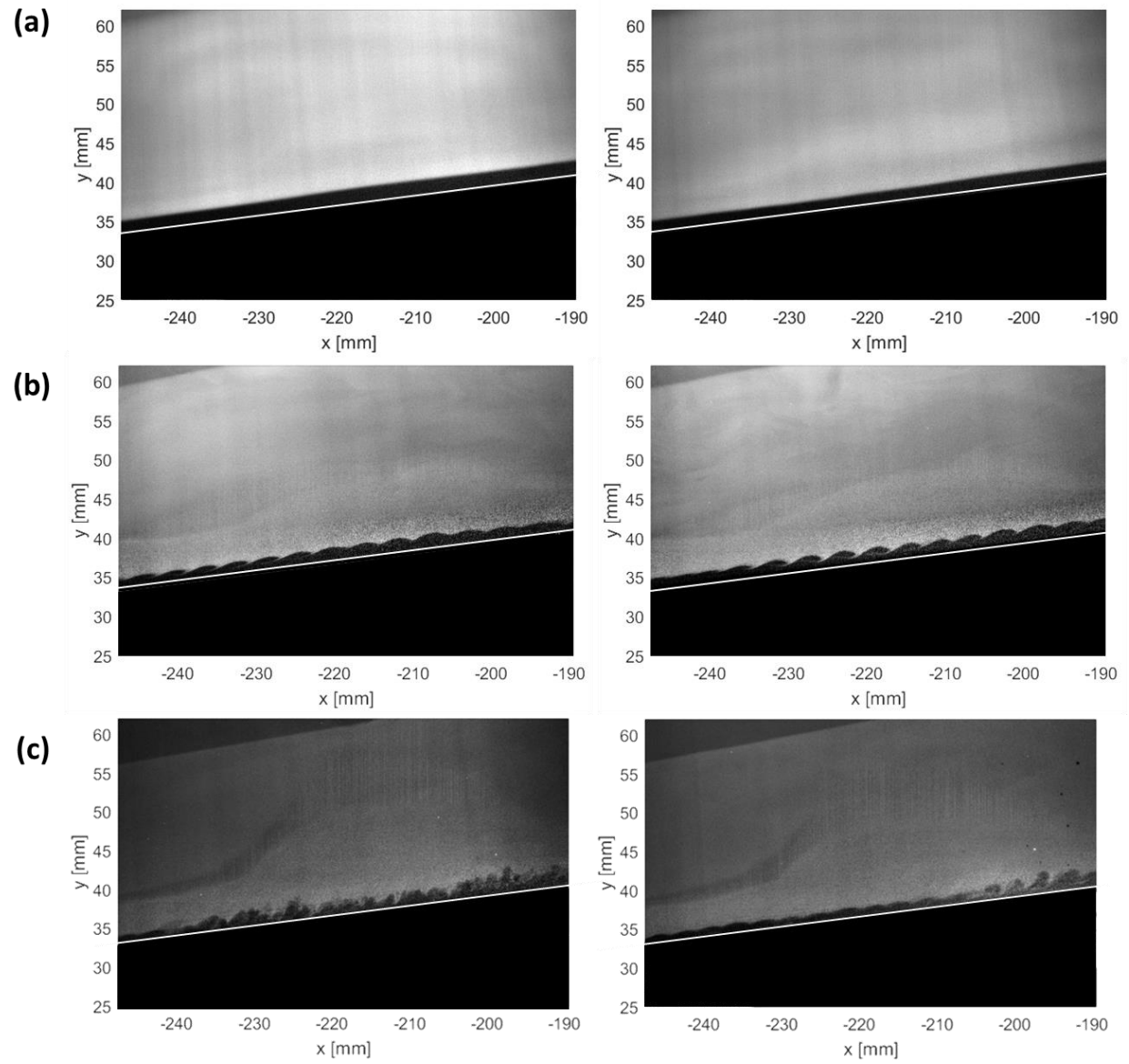

Fig. 3 Instantaneous frames of the boundary layer flow around a 7° half-angle cone for Re/m (a) 4×10^6, (b) 10×10^6, and (c) 14×10^6. Image columns show different frames in time. The solid white line indicates the surface of the model.

B. Near Wake Results

After verifying the CO_2 seeding system was operating as expected, it was used to visualize the near wake flow with PLS. Figure 4 shows instantaneous images of the wake behind the slender cone for the two lower Reynolds number cases, Runs 1 and 2. Image intensity discontinuities result in the PLS figures as a result of combining the images from two different cameras. The PLS images, Fig. 4(a) and 4(b), show that carbon dioxide particles condense and scatter light in the free stream, while the shear layer is noticeably darker due to evaporation of the particles. The expansion wave over the cone is also well-characterized by PLS. Figure 4(a) shows a predominantly laminar wake flow, consistent with the schlieren images in Fig. 4(c). With an increased Reynolds number, Fig. 4(b), second-mode waves are visible at the aft end of the model. These structures develop into large shear layer rollers downstream as the wake begins to transition to turbulence. Similar large-scale structures are also visible in the same locations of the schlieren images, Fig. 4(d), although the path-integrated nature of the schlieren obscures some of the turbulent features. For both conditions, turbulent structures within the wake are not visible with the current CO_2 seeding system, as no condensate remains after passing through the hot shear layer.

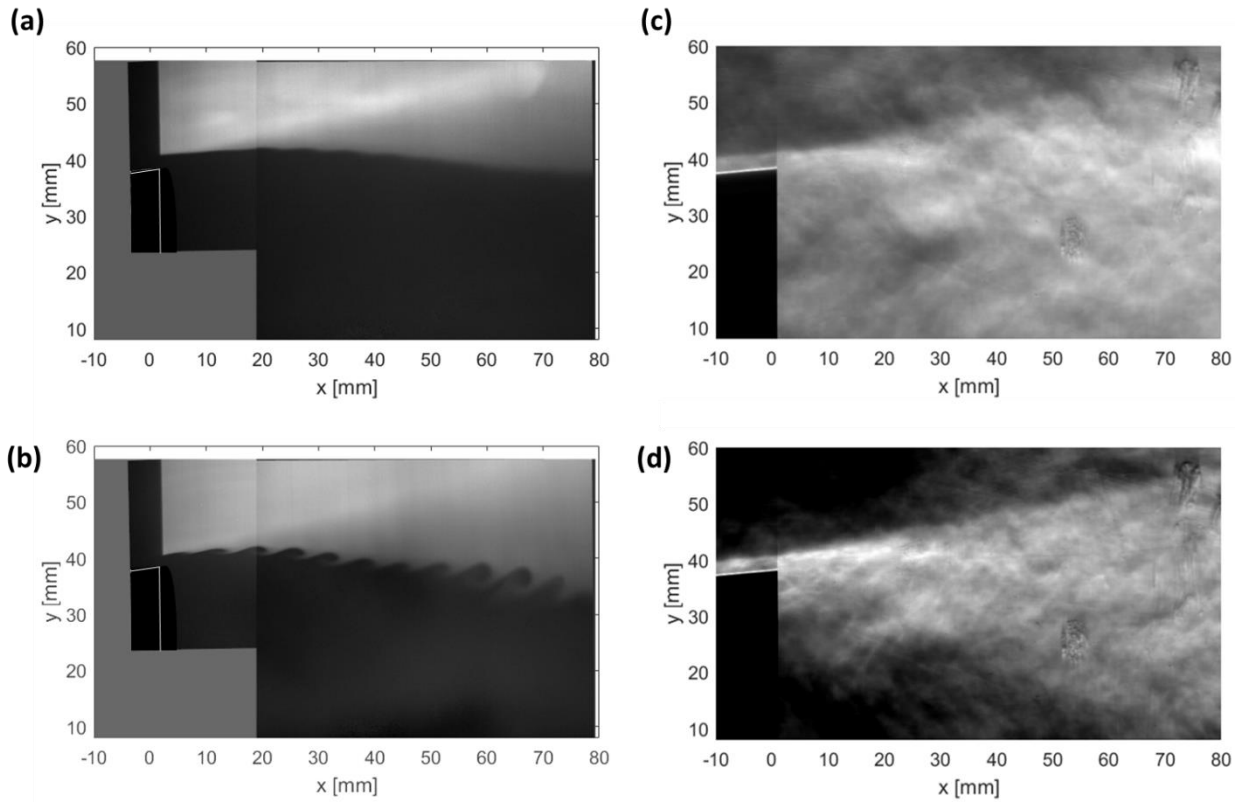

Fig. 4 Instantaneous images of the near wake visualized using PLS (a,b) and schlieren (c,d). Top row: Run 1, Re/m = 4 × 10^6. Bottom row: Run 2, Re/m = 7 × 10^6. The solid white line depicts the model surface.

Wake images at two higher Reynolds numbers, Runs 3 and 4, are shown in Fig. 5. Further increasing Reynolds number, in Fig. 5(a), the rolling structures do not dissipate, but instead develop into more finger-like turbulent structures downstream. The schlieren images, Fig. 5(c), show structures nearest to the model of similar size and frequency. In the highest Reynolds number case, Fig. 5(b), the flow structures appear highly turbulent immediately downstream of the base of the model. The schlieren images, Fig. 5(d), also reflect this highly turbulent wake structure, although the structures are more difficult to individually distinguish with this path-integrated measurement. Overall, the shear layer is well-characterized by the CO_2-enhanced Rayleigh scattering and flow structures are comparable for the PLS and schlieren images.

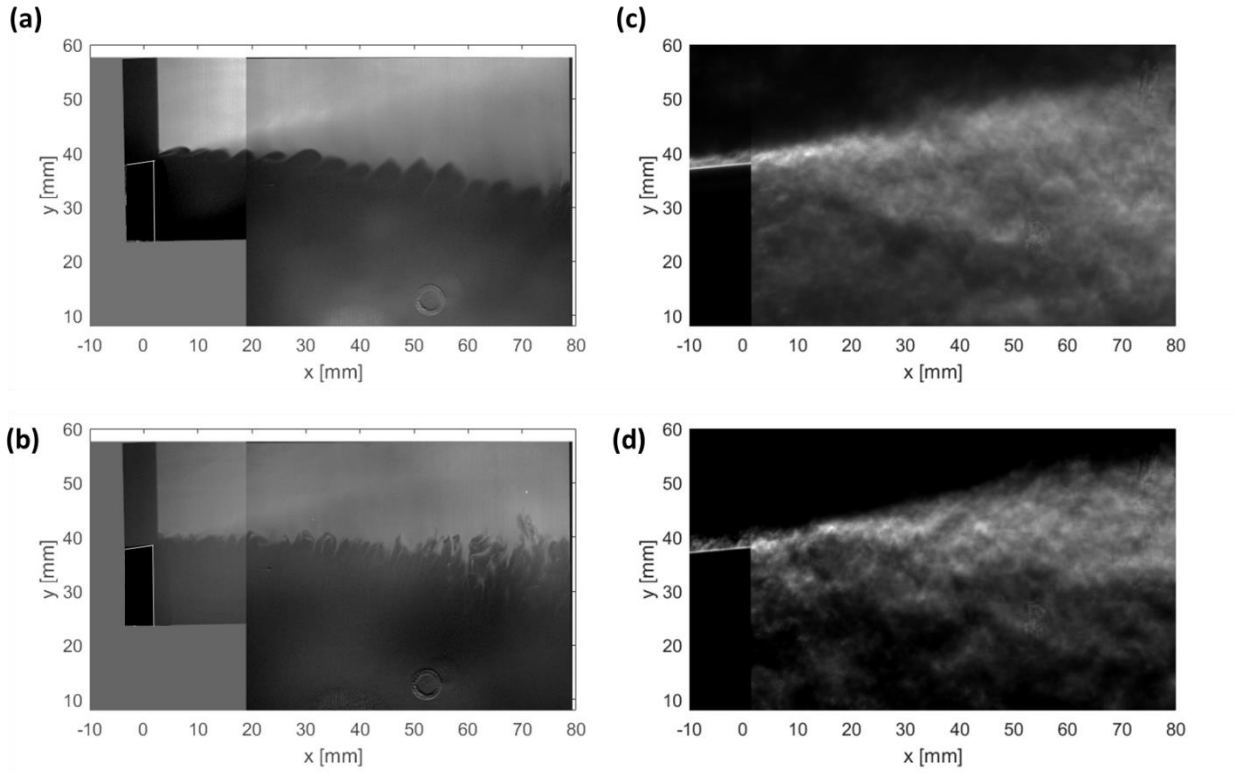

Fig. 5 Instantaneous images of the near wake visualized using PLS (a,b) and schlieren (c,d). Top row: Re/m = 10×10^6. Bottom row: Re/m = 14×10^6. The solid white line depicts the model surface.

C. Far Wake Results

In an additional measurement configuration, the PLS cameras were moved downstream to observe the far wake. Figure 6 highlights the image results for two different Reynolds numbers, Runs 2 and 3. The discontinuities of Fig. 6(a,b) are again the result of combining the images from two cameras, while the oblique lines on either side of the

images are boundaries of the laser sheet. The narrowest part of the wake, the neck, and the recompression shock are visible in the PLS images. A dark line can be seen in the schlieren images, Fig. 6(c,d), which distinguishes the recompression shock. Figure 6(a) has a similar structure to the near wake, with rolling structures dissipating further downstream in the neck region. For Run 3, Fig. 6(b), turbulent structures resembling shark fins are observed near the recompression shock. These "shark fin" structures were not visible in the near wake images or for other tunnel conditions. Comparing PLS to schlieren shows identical recompression shock locations; however, no fin-like turbulent features are visible. It is therefore suspected that these jagged structures are a result of a condensation shock from the CO_2. Condensation shocks from water in supersonic nozzles have been widely studied [22-24], but some studies have also observed CO_2 condensation shocks [25-27]. These shocks can occur when supersaturation is present in a wind tunnel flow. The flow can accept a maximum amount of heat addition from condensation. If flow conditions change enough for rapid condensation to occur, excess heat addition can result in a condensation shock, which is typically normal to the flow [23, 28]. The recompression shock may be disturbing the flow and causing the rapid condensation of supersaturated CO_2, as the shark fin structures only appear near this shock region. Future work will seek to investigate and mitigate this behavior by testing the CO_2 seeding system thoroughly at varying temperatures and Reynolds numbers. Reducing the amount of CO_2 but improving its visibility by suppressing the background using an iodine filter will also be investigated. Lastly, condensation shocks may be detectable using schlieren imaging while operating the CO_2 seeder.

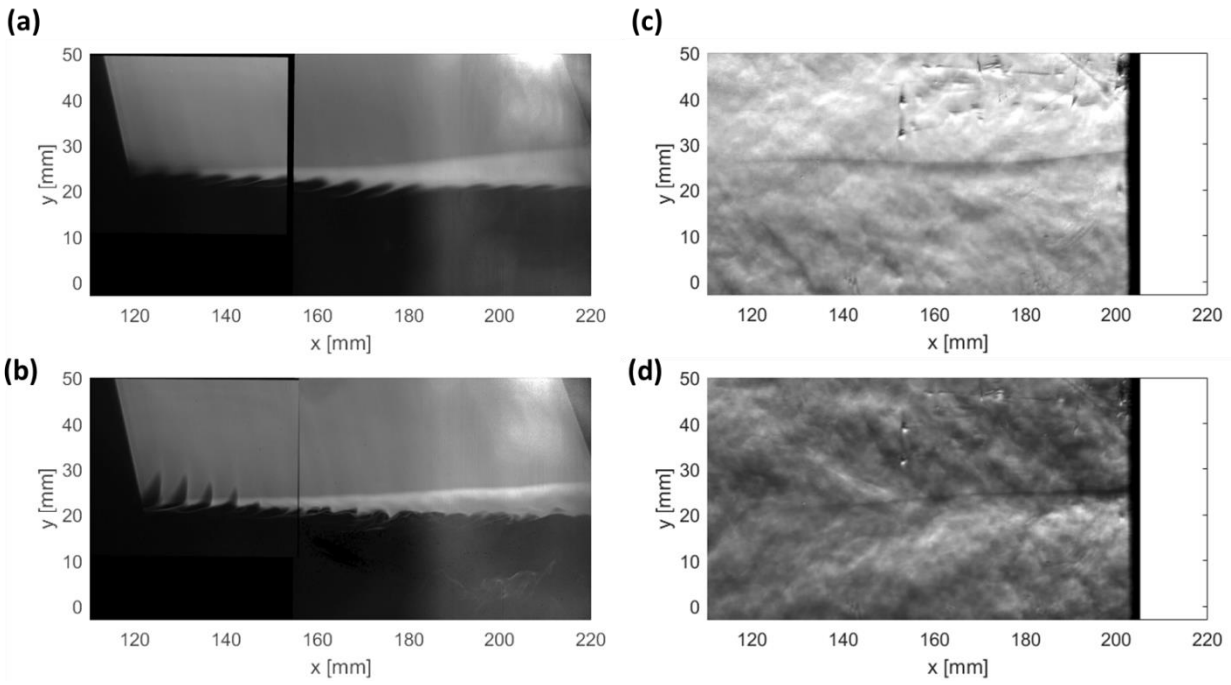

Fig. 6 Instantaneous images of the far wake visualized using PLS (a,b) and schlieren (c,d). Top row: Run 2, Re/m = 7 × 10^6. Bottom row: Run 3, Re/m = 10 × 10^6.

D. Signal Levels

To use the CO_2 seeding system to obtain quantitative FRS measurements inside the shear layer, some scattering signal needs to be detectable. Figure 7 shows false color average images from the CO_2-enhanced Rayleigh scattering to assess signal levels within the boundary layer flow. The rows are shown in increasing Reynolds number. The left column shows raw image intensities, with the background image subtracted. These figures serve to quantify how much signal is present solely due to the CO_2 light scattering. The right column of Fig. 7 shows the signal-to-noise ratio ($SNR = 10 \log_{10} \frac{P_{signal}}{P_{noise}}$; power, P) of the images, with noise estimated as the variance within the background images. These figures quantify how the signal images compare to background intensity, which is likely indicative of the quality of future FRS measurements.

In general, signal levels decrease with increasing Reynolds number. For Run 1, strong signal ($SNR > 10$) exists within the conical shock and boundary layer interface. For the higher Reynolds number runs, the signal is moderate within the shock. For all the background-subtracted images, Fig. 7(a), the signal is very low within the boundary layer, meaning no CO_2 has survived to scatter light in this region. In Fig. 7(b), strong background scattering is apparent due

to the laser sheet reflecting off the model surface. The signal levels within the boundary layer appear stronger in the *SNR* images, although this is likely due to the presence of the background scattering.

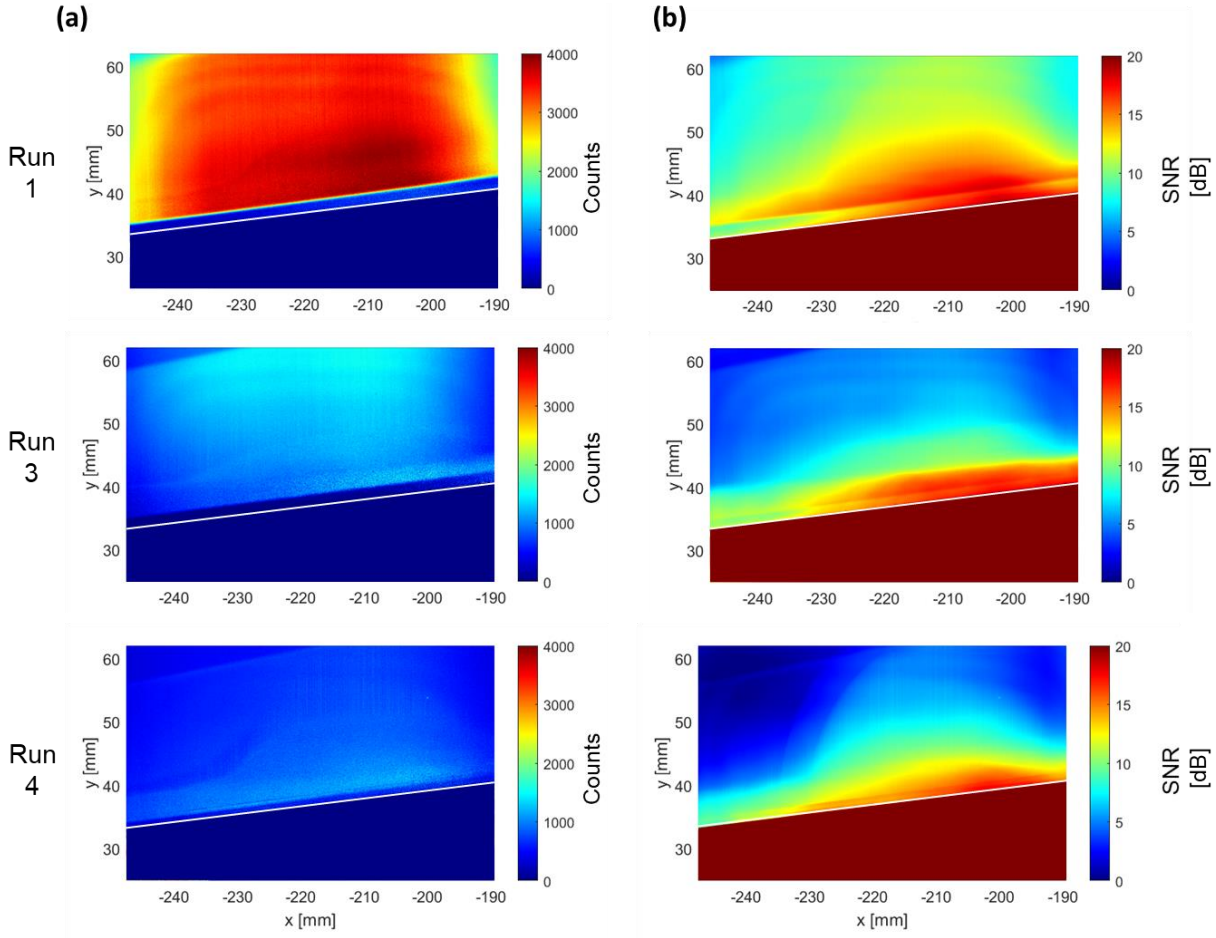

Fig. 7 Signal levels in the boundary layer shown for increasing Reynolds number (Runs 1, 3, and 4). (a) Background-subtracted images. (b) Raw images relative to background intensity (*SNR*). The solid white line indicates the surface of the model.

Average signal levels within the near wake are shown in Fig. 8. These signal levels are higher than in the boundary layer since the laser sheet is not reflecting off the model surface. In general, strong signal ($SNR > 10$) exists in the freestream and near the recompression shock for the two lowest Reynolds numbers. Moderate signal levels are also present within the shear layer and interface regions for these cases. For higher Reynolds numbers, the signals in the freestream and shock are much lower, meaning less CO_2 has condensed to scatter light. Although unapparent in the background-subtracted images, excess background light scattering can be seen to obscure the flow signal in the *SNR* images for these higher cases. The same trend was observed in the boundary layer images. These trends may indicate that less CO_2 condensate can form at these higher pressures, which could result in greater background scattering from

reflections on either side of the laser sheet. Very low scattering signal is seen within the wake, meaning little to no CO_2 has survived through the hotter shear layer for all measured cases.

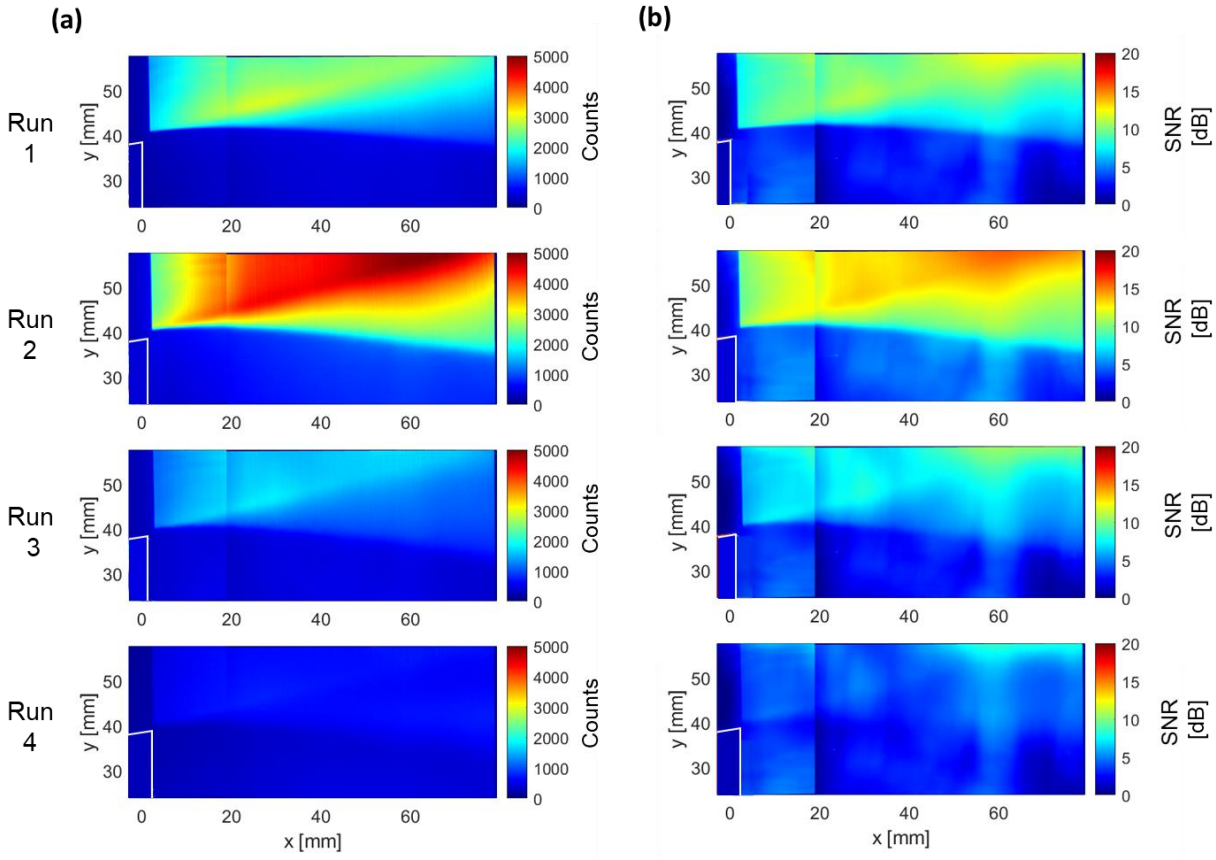

Fig. 8 Signal levels in the near wake shown for increasing Reynolds number (Runs 1 – 4). (a) Background-subtracted images. (b) Raw images relative to background intensity (*SNR*).

Insufficient scattering signal will likely make measurements in the boundary layer and wake challenging or nearly impossible. Some improvements to the CO_2 seeding system and measurement configuration are being considered to improve scattering signals within these regions. The enhanced Rayleigh scattering images shown by the current work did not use a molecular gas filter, which would reject background light based on its frequency. If the laser frequency is tuned to a region of high iodine absorption, background scattering does not experience a Doppler shift and is therefore suppressed. This suppression may help to extract any existing information within the wake flow. Additionally, modification to the seeding system may improve scattering performance. Supplying CO_2 using independent helium heads will help to maintain uniform flow seeding as the level of CO_2 in the bottles decreases throughout the duration of wind tunnel testing. Lastly, research on using alternative gases is being explored. Another

gas may exist which possesses the desired phase characteristics at tunnel operating conditions, and its condensation may survive hotter temperatures to survive in the wake. Alternatively, several early papers [21, 22, 29] on condensation in nozzles suggest that the addition of another gas may serve as nucleation sites for the CO_2, possibly allowing for the CO_2 to condense in fewer, larger particles, rather than a fine fog. It may therefore be possible for this condensed fog to survive through the temperature rise in the wake and produced higher scattering signals. Although ethanol or water are likely candidates for CO_2 "seed" nucleators, the previously mentioned safety concerns must be mitigated before this idea can be evaluated.

IV. Conclusions

The current work has described the implementation of the CO_2 seeder in Sandia's HWT. Carbon dioxide supplied by the seeding system condensed in the freestream, then evaporated in the higher temperature boundary layer and wake. The PLS boundary layer images showed details of second-mode waves transitioning into turbulence with higher Reynolds numbers. PLS images also revealed large-scale turbulent structures in the wake which increased in size downstream. With increasing Reynolds number, these structures progressed into longer, finger-like turbulence as the wake transitioned. Comparisons to schlieren images showed similar structures in the near wake, as well as identical locations of the wake neck and recompression shock. However, the planar enhanced Rayleigh scattering images better visualized details of the wake structure, compared to the path-integrated schlieren images, in which turbulent structures were barely discernible. Suspected condensation shocks were present for higher Reynolds numbers, showing fin-like turbulent structures in the far wake of the PLS images. While scattering signal levels in the freestream and shock regions appear suitable for quantitative measurements, signals within the boundary layer and wake were inadequate. Various modifications to the CO_2 seeding system and Rayleigh scattering measurement are being considered to try to improve scattering levels in the wake. However, the existing seeding system can provide planar details of the turbulence structure of the boundary layer and wake, valuable for many different applications. Overall, the successful performance of this CO_2 seeding system at various Reynolds numbers adds a new capability to the Sandia HWT, which can enable quantitative measurements, such as FRS, in the future.

Acknowledgments

Sandia National Laboratories is a multi-mission laboratory managed and operated by National Technology and Engineering Solutions of Sandia, LLC., a wholly owned subsidiary of Honeywell International, Inc., for the U.S. Department of Energy's National Nuclear Security Administration under contract DE-NA0003525. The views expressed in the article do not necessarily represent the views of the U.S. Department of Energy or the United States Government.

References

[1] Levensteins, Z., Krumins, M. "Aerodynamic Characteristics of Hypersonic Wakes," *AIAAJ* Vol. 5, No. 9, 1967, pp. 1596-1602.
doi: 10.2514/3.4256

[2] Boguszko, M., Elliott, G.S. "On the use of filtered Rayleigh scattering for measurements in compressible flows and thermal fields," *Experiments in Fluids* Vol. 38, 2005, pp. 33-49.
doi: 10.1007/s00348-004-0881-4

[3] Poggie, J., Erbland, P.J., Smits, A.J., Miles, R.B. "Quantitative visualization of compressible turbulent shear flows using condensate-enhanced Rayleigh scattering," *Experiments in Fluids* Vol. 37, 2004, pp. 438-454.
doi: 10.1007/s00348-004-0828-9

[4] Bourdon, C. J., Dutton, J.C. "Planar visualizations of large-scale turbulent structures in axisymmetric supersonic separated flows," *Physics of Fluids* Vol. 11, No. 1, 1999, pp. 201-213.
doi: 10.1063/1.869913

[5] Clemens, N. T., Mungal, M.G. "A planar Mie scattering technique for visualizing supersonic mixing flows," *Experiments in Fluids* Vol. 11, 1991, pp. 175-185.
doi: 10.1007/BF00190296

[6] Huntley, M., Smits, A. "Transition studies on an elliptic cone in Mach 8 flow using Filtered Rayleigh Scattering," *Eur J Mech B-Fluids* Vol. 19, 2000, pp. 695-706.
doi: 10.1016/S0997-7546(00)00130-8

[7] Smith, M. W., Smits, A.J. "Visualization of the structure of supersonic turbulent boundary layers," *Experiments in Fluids* Vol. 18, 1995, pp. 288-302.
doi: 10.1007/2FBF00195099

[8] Humble, R. A., Peltier, S.J., Bowersox, R.D.W. "Visualization of the structural response of a hypersonic turbulent boundary layer to convex curvature," *Physics of Fluids* Vol. 24, 2012, pp. 106103-1-24.
doi: 10.1063/1.4761833

[9] Crafton, J., Elliott, G., Carter, C., Beutner, T., Baust, H. "Filtered Rayleigh scattering velocimetry for wind tunnel applications." 2004, p. 189.

[10] McKenzie, R. L., Reinath, M.S., Jenkins, T.P. "Advances in Planar Doppler Velocimetry for Large-Scale Wind Tunnels," *24th AIAA Aerodynamic Measurement Technology and Ground Testing Conference*. Portland, Oregon, 2004, p. 25.

[11] Meyers, J. M., Lee, J.W., Cavone, A.A. "Boundary layer measurements in a supersonic wind tunnel using Doppler global velocimetry," *15th Intl Symp on App of Las Techniques to Fluid Mech*. Lisbon, Portugal, 2010, p. 11.

[12] Beresh, S. J., Casper, K.M., Wagner, J.L., Henfling, J.H., Spillers, R.W., Pruett, B.O. "Modernization of Sandia's Hypersonic Wind Tunnel," *53rd AIAA Aerospace Sciences Meeting*. Kissimmee, Florida, 2015, p. 15.

[13] Erbland, P. J., Baumgartner, M.L., Yalin, A.P., Etz, M.R., Muzas, B., Lempert, W.R., Smits, A.J., Miles, R.B. "Development of planar diagnostics for imaging Mach 8 flowfields using carbon dioxide and sodium seeding," *35th Aerospace Sciences Meeting & Exhibit*. Reno, Nevada, 1997.

[14] Zhang, C., Lee, C. "Rayleigh-scattering visualization of the development of second-mode waves," *J Vis* Vol. 20, 2017, pp. 7-12.
doi: 10.1007/s12650-016-0384-4

[15] Do, H., Im, S.K., Mungal, M.G., Cappelli, M.A. "Visualizing supersonic inlet duct unstart using planar laser Rayleigh scattering," *Experiments in Fluids* Vol. 50, 2011, pp. 1651-1657.
doi: 10.1007/s00348-010-1028-4

[16] Aguilera, C., Sosa, J., Hyde, E.W., Goodwin, G.B., Kessler, D.A., Hess, A.M., Miklosovic, D.S. "Characterization of Supersonic Wind Tunnel Flow Quality Using Planar Laser CO2 Rayleigh Scattering," *AIAA Propulsion and Energy 2021 Forum*. Virtual, 2021, p. 16.

[17] Casper, K. M., Beresh, S.J., Henfling, J.H., Spillers, R.W., Pruett, B.O., Schneider, S.P. "Hypersonic Wind-Tunnel Measurements of Boundary-Layer Transition on a Slender Cone," *AIAAJ* Vol. 54, No. 4, 2016, pp. 1250-1263.
doi: 10.2514/1.J054033

[18] Wegener, P. P., Clumpner, J.A., Wu, B.J.C. "Homogeneous Nucleation and Growth of Ethanol Drops in Supersonic Flow," *Physics of Fluids* Vol. 15, No. 11, 1972, pp. 1869-1876.
doi: 10.1063/1.1693796

[19] Dingilian, K. K., Halonen, R., Tikkanen, V., Reischl, B., Vehkamäki, Wyslouzil, B.E. "Homogeneous nucleation of carbon dioxide in supersonic nozzles I: experiments and classical theories," *Phys Chem Chem Phys* Vol. 22, 2020, pp. 19282-19298.
doi: 10.1039/d0cp02279a

[20] Wölk, J., Strey, R., Heath, C.H., Wyslouzil, B.E. "Empirical function for homogeneous water nucleation rates," *J Chem Phys* Vol. 117, No. 10, 2002, pp. 4954-4960.
doi: 10.1063/1.1498465

[21] Hill, P. G. "Condensation of water vapour during supersonic expansion in nozzles," *J Fluid Mech* Vol. 25, No. 3, 1966, pp. 593-620.
doi: 10.1017/S002211066000284

[22] Wegener, P. P. "Condensation Phenomena in Nozzles," *AIAA Heterogeneous Combustion Conference*. Palm Beach, Florida, 1963, p. 12.

[23] Wegener, P. P., Pouring, A.A. "Experiments on Condensation of Water Vapor by Homogeneous Nucleation in Nozzles," *Physics of Fluids* Vol. 7, No. 3, 1964, pp. 352-361.
doi: 10.1063/1.711206

[24] Matsuo, K., Kawagoe, S., Sonoda, K., Sakao, K. "Studies of Condensation Shock Waves (Part 1, Mechanism of their Formation)," *Bulletin of JSME* Vol. 28, No. 241, 1985, pp. 1416-1422.
doi: 10.1299/jsme1958.28.1416

[25] Bier, K., Theis, G. "Spontaneous condensation in stationary nozzle flow of carbon dioxide in a wide range of density," *IUTAM Symposium*. Göttingen, Germany, 1989, pp. 129-141.

[26] Lettieri, C., Paxson, D., Spakovszky, Z., Bryanston-Cross, P. "Characterization of Non-Equilibrium Condensation of Supercritical Carbon Dioxide in a de Laval Nozzle," *ASME Turbo Expo 2017: Turbomachinery Technical Conference and Exposition*. Charlotte, North Carolina, 2017, p. 13.

[27] Bolaños-Acosta, A. F., Restrepo, J.C., Simões-Moreira, J.R. "Two semi-analytical approaches for solving condensation shocks in supersonic nozzle flows," *International Journal of Heat and Mass Transfer* Vol. 173, No. 121212, 2021, p. 14.

[28] Pouring, A. A. "Thermal Choking and Condensation in Nozzles," *Physics of Fluids* Vol. 8, No. 10, 1963, pp. 1802-1810. doi: 10.1063/1.1761112

[29] Buckle, E. R., Pouring, A.A. "Effects of seeding on the condensation of atmospheric moisture in nozzles," *Nature* Vol. 208, No. 5008, 1965, pp. 367-369. doi: 10.1038/208367a0